

Discrimination of benign and malignant GGO in LIDC/IDRI dataset using three-dimensional oriented GLCM and hyper-surface fitting

Yasushi Hirano ¹ *, Rui Xu ¹, Rie Tachibana ²,
Shoji Kido ¹, and Hyoungeop Kim ³

¹ Graduate School of Medicine, Yamaguchi University, Japan

² Information Science and Technology Department, Oshima National College of Maritime Technology, Japan

³ Graduate School of Engineering, Kyushu Institute of Technology, Japan
yhirano@yamaguchi-u.ac.jp

Abstract. In this paper, the authors propose a novel method for texture analysis to discriminate malignant GGO from benign GGO in LIDC/IDRI dataset. The proposed method for texture analysis is based on the oriented gray level co-occurrence matrix (GLCM), which is also proposed by the authors. The oriented GLCM has the advantages that the noise reduction is unnecessary, and arbitrary direction and distance in the continuous space can be used because of the hyper-surface fitting. The authors discriminated tumors diagnosed as GGO in the LIDC/IDRI dataset into malignant or benign GGO. In the experiment, the proposed method classified 91 GGOs with 89% accuracy.

Keywords: Oriented GLCM, Texture analysis, GGO, Lung tumors, Differential diagnosis, LIDC/IDRI

1 Introduction

Discrimination between malignant and benign lung tumors in CT images for computer-aided diagnosis (CAD) is being actively investigated [1][2][3][4]. Lung tumors are clinically classified as solid, mixed, or ground-glass opacity (GGO). It is difficult to discriminate malignant GGO from benign GGO because of their pale intensity and ambiguous boundary. Although methods have been proposed to discriminate malignant GGO from benign GGO, they use high resolution CT (HRCT). However a more practical method is required that can be applied to thick CT images. A dataset of lung tumors has been published named the LIDC/IDRI (the Lung Imaging Database Consortium and Image Database Resource Initiative) dataset [5]. This dataset contains not only CT images but also

* This study is supported by MEXT KAKENHI Grant Number 21103008 and JSPS KAKENHI Grant Number 24700457. The authors acknowledge the National Cancer Institute and the Foundation for the National Institutes of Health, USA and their critical role in the creation of the free publicly available LIDC/IDRI Database used in this study.

the boundaries of tumors and annotations such as malignancy of the tumors and texture in the tumors. Because the LIDC/IDRI dataset has various values of pixel spacing and slice thickness of CT images, it is suitable to evaluate the performance of discrimination methods in actual situations.

This paper describes a novel method to calculate gray level co-occurrence matrix (GLCM) and its application to discriminate malignant GGO from benign GGO in CT images. In this method, three-dimensional (3D) gray images are locally converted into continuous functions using the hyper-surface fitting [6]. Then GLCM and texture features [7] are calculated using this continuous function. The obtained texture features are used to discriminate GGO. There is no need to reduce noise in the images because of the hyper-surface fitting. Furthermore, GLCM can be calculated in an arbitrary direction and an arbitrary distance.

The proposed method is based on texture features using GLCM and hyper-surface fitting. Texture features based on GLCM were originally proposed for the texture analysis for 2D images and then applied to 2D medical images [3][8][9]. GLCM for 3D images was proposed and applied to 3D medical images in the literatures [10][11]. However, because these methods were proposed for discrete images, the direction and the distance in the calculation of GLCM are also discrete. The method proposed in this paper solves these problems. Because GLCM and Haralick's features are still widely used in this field, it is thought that they have great ability to analyze texture and there is a great demand for them. But they have been used for 40 years with little expansion about dimensionality and normalization of the orientation of objects. Hence, the authors propose a novel GLCM.

Furthermore, the classification method based on the oriented GLCM was evaluated using LIDC/IDRI dataset, and sensitivity, specificity and accuracy of discrimination were 77%, 94% and 89%. For example, sensitivity, specificity and accuracy of the method proposed in the literature [1] were 100%, 48% and 56%, respectively. Comparing these two results, the performance of the proposed method in this paper is high enough.

2 Method

In the proposed method, the hyper-surface fitting at each voxel in the GGO region is performed to locally obtain a quadratic polynomial of three variables as the approximation of the CT image. Next, by using the coefficients of the obtained function, eigenvectors of Hessian matrix are calculated. Then, by using the CT value on the point of interest (POI) and that on the point in the direction of the eigenvector away from POI, GLCM is calculated. Finally, Haralick's texture features for discrimination are calculated using the GLCM. The flowchart of the proposed method is shown in Fig.1.

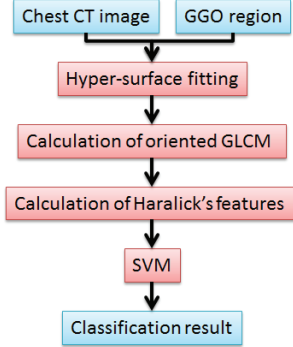


Fig. 1. Flowchart of proposed method

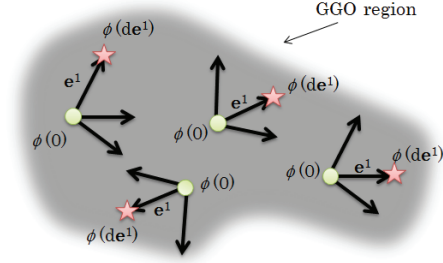


Fig. 2. Two sets of values (circles and stars) used to calculate oriented GLCM

2.1 Hyper-surface fitting

The hyper-surface fitting is a method to estimate values on voxels in the neighborhood of POI under a certain criterion [6]. Generally, the values on the voxels are expressed by a locally defined function. For example, we assume that the criterion is “the minimum square error criterion”, and a 3D gray discrete image $f(x, y, z)$ will be fitted using the following known continuous function

$$u = \phi(x, y, z; \mathbf{a}), \quad (1)$$

where $\mathbf{a} = (a_1, \dots, a_M)$ are unknown coefficients of variables in the function. The local square error between f and ϕ is given as

$$\epsilon_{i,j,k} = \sum_{(x,y,z) \in R_N(i,j,k)} \{f(x, y, z) - \phi(x, y, z; \mathbf{a})\}^2, \quad (2)$$

where $\sum_{(x,y,z) \in R_N(i,j,k)}$ means a summation on voxels in the neighborhood region $R_N(i, j, k)$ at the POI (i, j, k) , and POI can be the origin of the neighborhood region without loss of generality. To minimize this error, the $\epsilon_{i,j,k}$ is differentiated partially with a_m , ($m = 1, \dots, M$), and partial differentials are set to be 0 as follows,

$$\frac{\partial \epsilon_{i,j,k}}{\partial a_m} = -2 \sum_{(x,y,z) \in R_N(i,j,k)} \{f(x, y, z) - \phi(x, y, z; \mathbf{a})\} \frac{\partial \phi}{\partial a_m} = 0. \quad (3)$$

By solving these M equations, the M coefficients of the function ϕ are decided. The advantages of the hyper-surface fitting are as follows.

- Noise is reduced without applying any filters such as a Gaussian filter or a median filter.
- Because discrete images such as CT images are converted to continuous images, CT values on arbitrary locations can be obtained.

In the remaining part of this paper, the authors use a quadratic polynomial of three variables as the function ϕ . The coefficients of the polynomial are denoted as a_1 for the constant term, a_{x^2} for x^2 , and so on. Each POI has different values of coefficients.

2.2 Hessian matrix

The Hessian matrix is obtained using the second order partial differentials of the function ϕ as follows.

$$H = \begin{pmatrix} \frac{\partial^2 \phi}{\partial x^2} & \frac{\partial^2 \phi}{\partial x \partial y} & \frac{\partial^2 \phi}{\partial x \partial z} \\ \frac{\partial^2 \phi}{\partial y \partial x} & \frac{\partial^2 \phi}{\partial y^2} & \frac{\partial^2 \phi}{\partial y \partial z} \\ \frac{\partial^2 \phi}{\partial z \partial x} & \frac{\partial^2 \phi}{\partial z \partial y} & \frac{\partial^2 \phi}{\partial z^2} \end{pmatrix} \quad (4)$$

where $\frac{\partial^2 \phi}{\partial x^2}$, $\frac{\partial^2 \phi}{\partial x \partial y}$, etc. are the second derivatives of the function ϕ . Here, because POI is the origin of the neighborhood region in hyper-surface fitting, $\frac{\partial^2 \phi}{\partial x^2}$ at POI is

$$\frac{\partial^2 \phi}{\partial x^2} \Big|_{x=0, y=0, z=0}. \quad (5)$$

By re-substituting the polynomial obtained in Section 2.1 into Eq. (5),

$$\frac{\partial^2 \phi}{\partial x^2} \Big|_{x=0, y=0, z=0} = 2a_{x^2} \quad (6)$$

is obtained. In a similar fashion,

$$\frac{\partial^2 \phi}{\partial x \partial y} \Big|_{x=0, y=0, z=0} = \frac{\partial^2 \phi}{\partial y \partial x} \Big|_{x=0, y=0, z=0} = a_{xy}. \quad (7)$$

Thus, the Hessian matrix at POI is given as the following equation:

$$H = \begin{pmatrix} 2a_{x^2} & a_{xy} & a_{xz} \\ a_{xy} & 2a_{y^2} & a_{yz} \\ a_{xz} & a_{yz} & 2a_{z^2} \end{pmatrix}. \quad (8)$$

Because the entries in this Hessian matrix are obtained by the hyper-surface fitting, the eigenvalues and eigenvectors of the Hessian matrix are easily calculated. The authors denote the eigenvector as $\mathbf{e}^n = (e_x^n, e_y^n, e_z^n)^T$, ($n = 1, 2, 3$), which corresponds to the n -th greatest eigenvalue, and the eigenvectors are normalized so as that their norms are 1. The eigenvalues represent the magnitudes of the change of voxel values along the corresponding eigenvectors.

2.3 Estimation of CT value and calculation of the oriented GLCM

The CT value at the point d away from POI along with the direction \mathbf{e}^n is given as

$$\begin{aligned} \phi(d\mathbf{e}^n) = & a_{x^2}(de_x^n)^2 + a_{y^2}(de_y^n)^2 + a_{z^2}(de_z^n)^2 + \\ & a_{xy}de_x^n de_y^n + a_{yz}de_y^n de_z^n + a_{xz}de_x^n de_z^n + \\ & a_x de_x^n + a_y de_y^n + a_z de_z^n + a_1, \end{aligned} \quad (9)$$

and the estimated CT value at the POI is given as $\phi(0) = a_1$. By using these values, GLCM is calculated using all voxels in the GGO region defined by radiologists.

Assuming the gray level (bin) at the POI is α , and the gray level at a point in the direction \mathbf{t} and the distance d away from the POI is β , the authors denote the joint probability of α and β over the GGO region as $p(\alpha, \beta; \mathbf{t}, d)$ or $p(\alpha, \beta)$ if there is no confusion. The GLCM is a matrix composed of $p(\alpha, \beta)$ as the (α, β) -th entry of the matrix. In addition, each $p(\alpha, \beta)$ is normalized so that the summation of all $p(\alpha, \beta)$ in a GLCM is 1. Generally, both the direction \mathbf{t} and the distance d are discrete. The direction \mathbf{t} can be one of only four directions in a 2D case and 13 directions in a 3D case. In the proposed method, both the direction \mathbf{t} and the distance d are allowed to be continuous values by the hyper-surface fitting in Section 2.3. The authors use the eigenvectors \mathbf{e}^n of the Hessian matrix as the direction \mathbf{t} . Hence, the direction at each POI is different, but the GLCM is normalized by the direction of the eigenvector. Therefore, the authors named this GLCM the oriented GLCM. Fig. 2 shows the example of calculation of the oriented GLCM. The values $\phi(0)$ are used as the value at POIs (indicated with circles), and the values $\phi(d\mathbf{e}^1)$ are used as the values on the paired points (indicated with stars) of the POIs.

2.4 Texture features, feature selection, and classification

Haralick's texture features [7] are calculated using the oriented GLCM obtained in Section 2.3. Denoting N as the number of the gray levels and $p(\alpha, \beta)$ as the (α, β) -th entry in the oriented GLCM, the examples of calculation methods for Haralick's texture features are as follows.

$$(\text{Sum Entropy}) = - \sum_{\alpha=2}^{2N} p_{u+v}(\alpha) \log p_{u+v}(\alpha) \quad (10)$$

$$(\text{Entropy}) = - \sum_{\alpha=1}^N \sum_{\beta=1}^N p(\alpha, \beta) \log p(\alpha, \beta) \quad (11)$$

where $p_{u+v}(\gamma) = \sum_{\alpha=1}^N \sum_{\beta=1}^N p(\alpha, \beta)$, $(\alpha + \beta = \gamma, \gamma = 2, 3, \dots, 2N)$. There are 14 Haralick's texture features in all [7]. In this paper, 252 features (= 14 Haralick's features \times 3 directions \times 6 distances ($d = 1, 2, \dots, 6mm$ in plain scale)) are calculated. The elements of the direction \mathbf{t} and the distance d can be arbitrary real numbers with no relation to the pixel spacing or slice thickness of the original CT image, because the CT image is converted to local continuous functions by using the hyper-surface fitting. Then, some features that have high correlation with the ground truth are selected. By using the selected features, GGOs are classified into malignant GGO or benign GGO by a support vector machine (SVM) [12]. The kernel function is radial basis function (RBF), and the parameters of the kernel function are decided by using a grid search.

3 Experiments

3.1 Materials

Annotations about tumors contained in the LIDC/IDRI dataset are given by at most four radiologists. The annotations include the boundaries, malignancy, and texture. The authors classified tumors diagnosed as 1 (Highly Unlikely for Cancer) or 2 (Moderately Unlikely for Cancer) in “likelihood of malignancy” by over half the radiologists as “benign”, 4 (Moderately Suspicious for Cancer) or 5 (Highly Suspicious for Cancer) in “likelihood of malignancy” as “malignant”, and 1 (Non-Solid/Ground Glass Opacity) or 2 in “internal texture” as GGO. The number of GGOs used is 91 from 74 cases. These tumors contain 26 malignant GGOs, and 65 benign GGOs. The authors used logical OR of the tumor regions decided by radiologists as GGO regions.

Table 1 shows the variation of CT images used in this experiment from the perspective of the pixel spacing and the slice thickness. Because these CT images have a large variety of pixel spacing and slice thickness, discriminating between benign and malignant GGOs is a challenging problem.

Table 1. Frequency of cases used in this experiment from the perspective of pixel spacing and slice thickness

		Pixel spacing [<i>mm</i>]			
		0.5-0.6	0.6-0.7	0.7-0.8	0.8-0.9
Slice thickness [<i>mm</i>]	0.5-1.0	0	15	9	2
	1.0-1.5	4	10	17	1
	1.5-2.0	0	9	4	0
	2.0-2.5	2	6	7	2
	2.5-3.0	1	1	1	0

3.2 Feature selection

First, correlation coefficients between the ground truth (malignant GGO:1 and benign GGO: -1) and each of 252 features were calculated, where the features were normalized so that they were distributed between -1 and 1 . The method of calculation of the correlation coefficients is a method similar to the training phase of a kind of supervised machine learning methods. Then, 10 features were selected in descending order of correlation coefficients. Finally, the combination of features that achieved the best accuracy was decided from any combinations consist of features from the 10 features. The selected features were the entropy with $d = 6$ and the direction \mathbf{e}^2 , and entropy with $d = 5$ and the direction \mathbf{e}^1 . The correlation coefficients were 0.461 and 0.457, respectively.

3.3 Experimental results

The performance of the proposed method was evaluated by using a leave-one-out method. The confusion matrix is shown in Table 2, and the sensitivity, specificity and classification accuracy were 77%, 94% and 89%, respectively. The characters “M” and “B” in Table 2 mean “Malignant” and “Benign”, respectively. Figs. 3 and 4 show all misclassified malignant and benign GGOs, respectively.

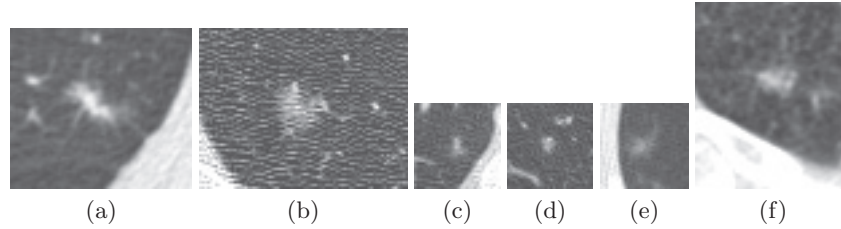


Fig. 3. Misclassified malignant GGO

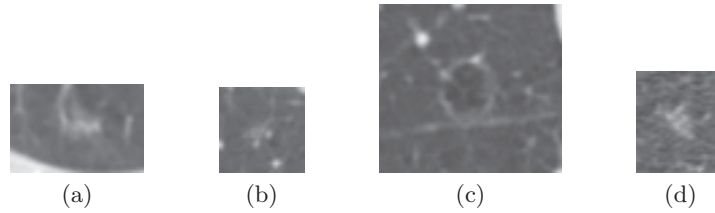


Fig. 4. Misclassified benign GGO

Table 2. Confusion matrix

		Proposed method	
		M	B
Radiologist	M	20	6
	B	4	61

Table 3. Frequency of misclassified cases from the perspective of pixel spacing and slice thickness

		Pixel spacing [mm]			
		0.5-0.6	0.6-0.7	0.7-0.8	0.8-0.9
Slice thickness [mm]	0.5-1.0	0	1	1	0
	1.0-1.5	0	2	2	0
	1.5-2.0	0	1	1	0
	2.0-2.5	0	0	2	0
	2.5-3.0	0	0	0	0

4 Discussion

When comparing misclassified GGOs (Figs.3 and 4) and correctly classified GGOs (Fig.5), there is a tendency to misclassify GGOs that are small or non-

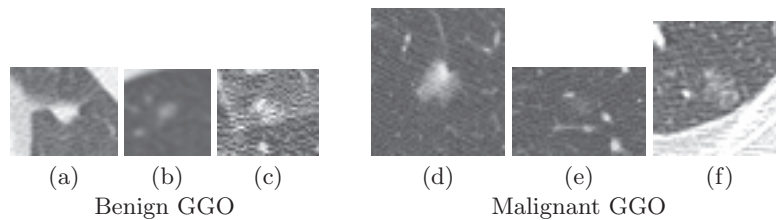


Fig. 5. Examples of correctly classified GGO

uniform in internal texture. Because these situations destabilize directions of eigenvectors, Haralick's features are also unstable. Additionally, GGOs that have very low CT values (Fig.4(a)(b) and Fig.5(e)) tend to be classified into malignant GGO, even if they are actual malignant GGOs or not. The almost same problem occurs in GGO that has a cavity (Fig.4(c)). The CT values in this GGO itself has relatively high, but almost all portion of the computational region is in a cavity. To solve these problems, optimization of parameters in the classifier and/or addition of features are required. Especially, the performance can be higher if other features are used complementally.

On the other hand, the proposed method is insusceptible to noise (Fig.5(c)(f)). It is thought that the hyper-surface fitting works effectively to reduce noise.

If Tables 1 and 3 are compared, the ability of classification of the proposed method is less related with the pixel spacing or the slice thickness of the CT images. Therefore, it is thought that the proposed method will be practical in the actual situation.

5 Conclusion

In this paper, the authors proposed a novel method to discriminate malignant GGO from benign GGO in CT images that have various pixel spacing and slice thickness. The features were calculated using hyper-surface fitting and the oriented GLCM that was also proposed by the authors. The sensitivity, specificity and accuracy of discrimination between malignant and benign GGO using LIDC/IDRI dataset were 77%, 94% and 89%, respectively.

The future works include improvement of the feature selection method by using a more common method, combination with other features [13], and discrimination using GGO regions extracted automatically [14][15].

References

1. Suzuki K, Li F, Sone S, Doi K: Computer-aided diagnostic scheme for distinction between benign and malignant nodules in thoracic low-dose CT by use of massive training artificial neural network, *IEEE Trans. on Medical Imaging*, Vol.24, Issue 9, pp.1138–1150 (2005)

2. El-Baz A, Gimel'farb G, Falk R, El-Ghar M: Appearance analysis for diagnosing malignant lung nodules, 2010 IEEE International Symposium on Biomedical Imaging, pp.193–196 (2010)
3. Wanga H, Guoa XH, Jiaa ZW, Lib HK, Liangc ZG, Lic KC, Hed Q: Multilevel Binomial Logistic Prediction Model for Malignant Pulmonary Nodules Based on Texture Features of CT Image, *European Journal of Radiology*, Vol.74, Issue 1, pp.124–129 (2010)
4. Minami K, Kawata Y, Niki N, Ohmatsu H, Mori K, Yamada K, Eguchi K, Kaneko M, Moriyama N: Classifying pulmonary nodules using dynamic enhanced CT images based on CT number histogram, *Proc. SPIE 6915, Medical Imaging 2008*, 69152P, (2008)
5. Armato SG III, McLennan G, Bidaut L, McNitt-Gray MF, Meyer CR, Reeves AP, Zhao B, Aberle DR, Henschke CI, Hoffman EA, Kazerooni EA, MacMahon H, van Beek EJR, Yankelevitz D, et al.: The Lung Image Database Consortium (LIDC) and Image Database Resource Initiative (IDRI): A completed reference database of lung nodules on CT scans, *Medical Physics*, Vol.38, pp.915–931 (2011)
6. Monga O and Benayoun S: Using partial derivatives of 3D images to extract typical surface features, *Rapport De Recherche Inria*, RR-1599 (1992)
7. Haralick RM, Shanmugam K, Dinstein I: Textural Features for Image Classification, *IEEE Trans. on Systems, Man and Cybernetics*, Vol.SMC-3, Issue 6, pp.610-621 (1973)
8. Hu W, Li H, Wang C, Gou S, Fu L: Characterization of collagen fibers by means of texture analysis of second harmonic generation images using orientation-dependent gray level co-occurrence matrix method, *J. Biomed. Opt.* Vol.17, No.2, Article ID 026007 (2012)
9. Anand SKV: Segmentation Coupled Textural Feature Classification for Lung Tumor Prediction, *IEEE International Conference on Communication Control and Computing Technologies (ICCCCT)*, pp.518–524 (2010)
10. Liu S, Cai W, Wen L, Eberl S, Fulham MJ, Feng D: A robust volumetric feature extraction approach for 3D neuroimaging retrieval, *IEEE International Conference of Engineering in Medicine and Biology Society (EMBC)*, pp.5657–5660 (2010)
11. Kovalev VA, Kruggel F, Gertz HJ, Cramon DY: Three-dimensional texture analysis of MRI brain datasets, *IEEE Trans. on Medical Imaging*, Vol.20, Issue 5, pp.424–433 (2001)
12. Chang CC and Lin CJ: LIBSVM : a library for support vector machines. *ACM Transactions on Intelligent Systems and Technology*, Vol.2, No.3, Article No.27, pp.1–27 (2011)
13. Hirano Y, Hasegawa J, Toriwaki J, Ohmatsu H, and Eguchi K: Interactive method to extract tumor regions from chest X-Ray CT images and its application to benign/malignant discrimination. *Systems and Computers in Japan*, Vol.36, No.8, pp.90-101 (2005)
14. Tachibana R, Kido S: Automatic segmentation of pulmonary nodules on CT images by use of NCI lung image database consortium. *Proc. SPIE 61440, Medical Imaging 2006*, 61440M (2006)
15. Tachibana R, Kido S, Hirano Y, Xu R : Reliability evaluation of radiologist and semiautomatic segmentation algorithm for small pulmonary nodules. *Proc. 97th Scientific Assembly and Annual Meeting of Radiological Society of North America (RSNA 2011)*, p.150 (2011)